

RESEARCH

Open Access



Neutrophil extracellular trap-derived double-stranded RNA aggravates PANoptosis in renal ischemia reperfusion injury

Shaoyong Zhuang^{1†}, Fangzhou Li^{1,3†}, Liya Wang^{4†}, Zilong Lai^{1†}, Dawei Li¹, Haoyu Wu¹, Jiajin Wu¹, Junwen Qu¹, Xianyun Zhang^{2*}, Ming Zhang^{1*}, Ruoyang Chen^{1*} and Xiaodong Yuan^{1*}

Abstract

A dysregulated inflammatory response and inflammation-associated cell death are central features of renal ischemia-reperfusion injury (IRI). PANoptosis, is a recently recognized form of inflammatory programmed cell death characterized by key features of pyroptosis, apoptosis and necroptosis; however, the specific involvement of PANoptosis in renal IRI remains unknown. By using neutrophil extracellular trap (NETs)-depleted *Pad4*^{-/-} mice, we found that NETs are essential for exacerbating tissue injury in renal IRI. Single-cell RNA sequencing (scRNA-seq) revealed that IRI promoted PANoptosis signalling in proximal tubular epithelial cells (PTs), whereas PAD4 knockout inhibited PANoptosis signalling. PTs expressed mainly RIPK1-PANoptosomes, which executed NET-induced PANoptosis in PTs in renal IRI model mice. Mechanistically, NET-derived double-stranded RNA (dsRNA) promoted PANoptosis in PTs, and PT-expressed TLR3 was responsible for the sensing the extracellular dsRNA. Treating mice with chemical inhibitors of the dsRNA/TLR3 complex suppressed PANoptosis and alleviated tissue injury in renal IRI. Together, the results of this study reveal a mechanism by which the NET-dsRNA-TLR3 axis aggravates PT cell PANoptosis in renal IRI.

[†]Shaoyong Zhuang, Fangzhou Li, Liya Wang and Zilong Lai have contributed equally to this work.

*Correspondence:

Xianyun Zhang
xyz197681@163.com
Ming Zhang
drmingzhang@126.com
Ruoyang Chen
chenrysju@163.com
Xiaodong Yuan
sduyuanxd@126.com

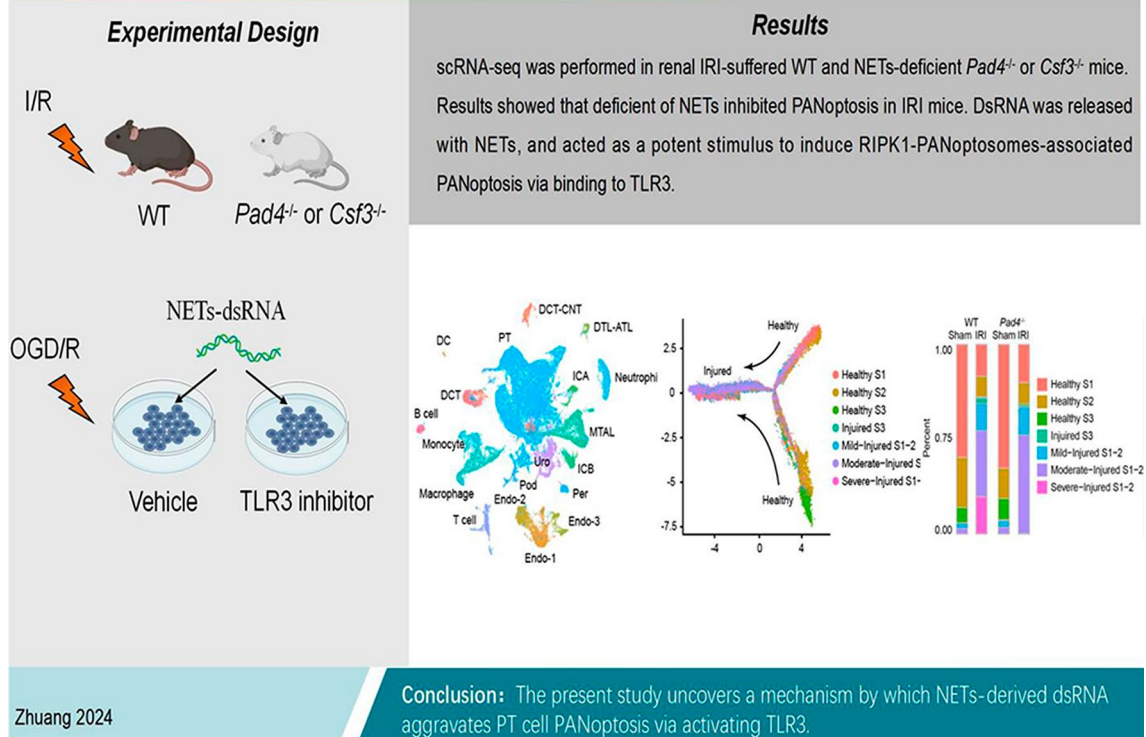
Full list of author information is available at the end of the article



© The Author(s) 2025. **Open Access** This article is licensed under a Creative Commons Attribution-NonCommercial-NoDerivatives 4.0 International License, which permits any non-commercial use, sharing, distribution and reproduction in any medium or format, as long as you give appropriate credit to the original author(s) and the source, provide a link to the Creative Commons licence, and indicate if you modified the licensed material. You do not have permission under this licence to share adapted material derived from this article or parts of it. The images or other third party material in this article are included in the article's Creative Commons licence, unless indicated otherwise in a credit line to the material. If material is not included in the article's Creative Commons licence and your intended use is not permitted by statutory regulation or exceeds the permitted use, you will need to obtain permission directly from the copyright holder. To view a copy of this licence, visit <http://creativecommons.org/licenses/by-nc-nd/4.0/>.

Graphical Abstract

Neutrophil extracellular traps-derived double-stranded RNA aggravates PANoptosis in renal ischemia reperfusion injury



Introduction

Ischemia-reperfusion injury (IRI) remains one of the most challenging problems in acute kidney injury [1]. Previous studies have shown that various forms of programmed cell death can be observed in renal IRI, including ferroptosis, pyroptosis, apoptosis and necroptosis [2, 3]. Programmed cell death may cause kidney injury directly or through the recruitment of immune cells and aggravation of inflammatory responses [4]. Therapeutic approaches that target programmed cell death can prevent the aberrant kidney epithelial cell death as well as the renal inflammation observed in IRI [2]. PANoptosis is a unique inflammatory programmed cell death pathway, that integrates the characteristics of pyroptosis, apoptosis and necroptosis [5]. Cytosolic innate immune sensors and regulators, such as ZBP1, AIM2 and RIPK1, recognize multiple pathogen-associated molecular patterns (PAMPs) and damage-associated molecular patterns (DAMPs) and promote the assembly of PANoptosomes to drive PANoptosis [6]. Accumulating evidence has revealed that PANoptosis can be observed in various inflammation-associated diseases, including infections, autoimmune diseases, IRI and cancer [7, 8]. PANoptosis not only contributes to the death of cells, but also

exacerbates inflammatory responses [9]. PANoptosis may be a potential target for renal IRI. However, the detailed mechanism by which PANoptosis is initiated in renal IRI and the specific approaches to target PANoptosis in the context of renal IRI remain unknown.

Neutrophils are the most abundant immune cells in human blood, and constitute the first-line responders in inflammation [10]. In renal IRI, neutrophils play key roles in inflammatory responses and subsequent tissue injury [11]. Neutrophil extracellular traps (NETs) are extracellular web-like structures composed of cytosolic and granule proteins that are assembled on a scaffold of decondensed chromatin [12]. Since they were first discovered, NETs have been shown to participate in the initiation of inflammatory responses in various diseases, including sepsis, inflammatory bowel diseases, and autoimmune diseases [12, 13]. Studies from our group and others have shown that NETs are essential in the pathological process of renal IRI [14, 15]. However, the specific mechanisms by which NETs induce inflammatory responses and cell death in renal IRI remain largely unclear.

In the present study, single-cell RNA sequencing (scRNA-seq) was used to compare the transcriptional differences between the kidneys of IRI model wild-type

(WT) and NET-deficient *Pad4*^{-/-} mice. We observed that NET deficiency markedly reduced the expression of injury markers in proximal tubular epithelial cells (PTs). Functional enrichment analysis revealed that pyroptosis, apoptosis and necroptosis signalling were suppressed in *Pad4*^{-/-} mice. Further mechanistic analysis indicated that NET-derived double-stranded RNA (dsRNA) aggravated PANoptosis in renal IRI by activating TLR3. Targeting the NET-dsRNA-TLR3 axis to inhibit PANoptosis may provide a potential approach for treating renal IRI.

Methods

Animal model

All animal experiments were performed in accordance with the National Institutes of Health Guide for the Care and Use of Laboratory Animals. *Csf3r*^{+/-} and *Pad4*^{+/-} mice were purchased from Cyagen Biosciences. Homozygous *Csf3r*^{-/-} and *Pad4*^{-/-} mice, and their WT littermates were used in the present study. The mice (male, 8–10 weeks old) were anesthetized with pentobarbital sodium and placed on a heating table. The mice were randomly grouped using a random number generator. IRI surgery was performed as previously reported [14]. Briefly, the mice were first subjected to right nephrectomy. The left renal pedicle was then clamped for 25 min. Sham controls underwent the same surgical procedures but without vascular occlusion. Twenty-four hours after surgery, the animals were sacrificed, and blood and renal tissue were collected. Inhibitors of pyroptosis (disulfiram, 50 mg/kg, MCE), apoptosis (Z-VAD-FMK, 3 mg/kg, MCE), necroptosis (necrosulfonamide, 10 mg/kg, MCE), RIPK1 (necrostatin 1 S, 6 mg/kg, MCE) and TLR3 (CU-CPT 4a, 6 mg/kg, MCE) were intraperitoneally injected ten minutes before surgery.

Single-cell RNA sequencing (scRNA-seq)

Kidney samples were minced into 1mm [3] cubes, and digested with DNase I and collagenase IV in RPMI 1640 for 30 min at 37°C. Then, 10% fetal bovine serum (FBS) was added to stop the reaction. After being filtered through a 40-µm cell strainer, the mixture was centrifuged at 800×g for 5 min, and lysis buffer was used to lyse the red blood cells. A countess II Automated Cell Counter (Thermo Fisher) was used to analyse the number and viability of the cells, and samples with a viability greater than 80% were considered qualified samples. Then, scRNA-seq of single-cell suspensions was performed by Shanghai Biotechnology Corporation. The cell suspensions were loaded onto a microfluidic chip to generate a complementary deoxyribonucleic acid (cDNA) library using a commercial 10x Genomics platform (10x Genomics). Beads with unique molecular identifiers (UMIs) and cell barcodes were loaded close to saturation, so that each cell was paired with a bead in a gel beads-in-emulsion

(GEM). After treatment with cell lysis buffer, polyadenylated RNA molecules hybridize to the beads. The beads were transferred to a single tube for reverse transcription. For cDNA synthesis, each cDNA molecule was tagged on the 5' end (that is, the 3' end of a messenger RNA transcript) with a UMI and a cell label indicating its cell of origin. The 10× beads were then subjected to second-strand cDNA synthesis, adaptor ligation, and universal amplification. The sequencing libraries were prepared via the use of randomly interrupted whole-transcriptome amplification products to enrich the 3' end of the transcripts linked with the cell barcode and UMI. All the remaining procedures, including library construction, were performed according to the standard manufacturer's protocol (CG000206 RevD).

Bioinformatics analyses were performed as previously described [18]. We excluded cells with fewer than 200 or more than 6000 detected genes (where each gene had to have at least one UMI aligned in at least three cells). The expression of mitochondrial genes was calculated using PercentageFeatureSet function of the Seurat package (v.4.0.3). To remove low-activity cells, cells whose expression of mitochondrial genes was greater than 10% were excluded. Doublet-like cells were identified using DoubletFinder (v.2.0.3). The normalized data was performed for extracting a subset of variable genes. Variable genes were identified while controlling for the strong relationship between variability and average expression. Next, we integrated data from different samples after identifying 'anchors' between datasets using FindIntegrationAnchors and IntegrateData in the Seurat package. Principal component analysis (PCA) was performed, and we reduced the data to the top 30 PCA components after scaling the data. Clusters on a 2D map were generated using uniform manifold approximation and projection (UMAP). The cells were clustered with the Louvain Method using the reduced PCA data with after a shared nearest neighbour graph was computed. For subclustering, we applied the same procedure of scaling, dimensionality reduction, and clustering to the specific set of data. For each cluster, we used the Wilcoxon rank-sum test to find significantly differentially expressed genes when the remaining clusters were compared. SingleR and known marker genes were used to identify cell types. To construct a single-cell pseudotime trajectory and illustrate potential cellular differentiation routines, the Monocle2 (v.2.4.0) algorithm was applied to PT.

Histological examination

Kidney tissues were harvested and fixed with 4% formaldehyde, embedded in paraffin, and sectioned at a thickness of 5 µm. Haematoxylin and eosin (H&E) and periodic acid-Schiff (PAS) staining were performed routinely. To evaluate the tubular injury score, 10 random

nonoverlapping high-power fields of H&E- and PAS-stained tissue sections per mouse were assessed by a pathologist, and the sections were semiquantitatively scored as follows: 0, no damage; 1, < 25%; 2, 25 to ~50%; 3, 50 to ~75%; and 4, > 75%.

Neutrophil isolation and activation

Neutrophils were isolated from mouse bone marrow using a mouse neutrophil isolation kit (Miltenyi) following the manufacturer's instructions. Neutrophils were cultured with RPMI 1640 (Gibco) supplemented with 10% FBS. NET formation was stimulated by incubating neutrophils with PMA (1 μ M, Sigma) for 6 h. To isolate NETs, the supernatant was discarded carefully, and NETs that had adhered to the bottom of the plate were washed 5 times with ice-cold PBS. After centrifugation at 1000 \times g for 5 min, NETs in the supernatant were collected. Neutrophil degranulation was induced by stimulation with fMLP (1 μ M, Sigma) for 2 h. After centrifugation at 500 \times g for minutes, the supernatant that containing the degranulation substrate was collected.

Immunohistochemical and Immunofluorescence staining

Kidney tissues were harvested and fixed with 4% formaldehyde, embedded in paraffin, and sectioned at a thickness of 5 μ m. Paraffin-embedded sections were dewaxed using a gradient ethanol series, heated in citrate-based buffer for antigen retrieval, and blocked with 3% H₂O₂ followed by 10% BSA. For immunohistochemical staining, antibodies against Ly6G (1:200, Abcam), C-Caspase-1 (1:200, CST), C-Caspase-3 (1:200, CST), P-MLKL (1:200, Invitrogen), and secondary antibody (1:2000, Abcam) were used, and the samples were stained using the reagents in a DAB substrate kit (Abcam). For immunofluorescence staining of renal tissues, an anti-Ly6G antibody (1:200, Abcam), an anti-CitH3 antibody (1:200, Abcam), and the appropriate secondary antibody (1:2000, Abcam) were used, and the samples were mounted with DAPI-containing mounting medium. Images were acquired with a confocal microscope (Leica). NETs expression in renal sections was calculated as CitH3. For in vitro immunofluorescence staining of NETs, neutrophils were stimulated with 1 μ M PMA for 6 h to induce the generation of NETs. NETs were fixed with 4% paraformaldehyde and treated with membrane permeabilization 0.1% Triton X-100. RNase T1 (40 U/mL, Thermo), RNase III (40 U/mL, Thermo), and DNase I (2 μ g/mL, Sigma) were incubated with NETs in PBS containing 5 mM MgCl₂ at 37 °C for 30 min. CitH3 antibody (1:200, Abcam), a dsRNA J2 antibody (1:200, Jena), and the appropriate secondary antibody (1:2000) were used, and the sections were mounted with DAPI-containing mounting medium. NETs were observed with a confocal microscope (Leica).

Cell culture

The renal tubular epithelial cell (TEC) line was a generous gift from Professor Xuemei Zhang (School of Pharmacy, Fudan University, Shanghai, China). Murine renal TECs were cultured in DMEM (Gibco) supplemented with 10% FBS (Gibco), in the presence of streptomycin and penicillin. The cells were subjected to oxygen glucose deprivation and reoxygenation (OGD/R) to mimic IRI in vitro as previously reported [16]. Briefly, TECs were cultured in glucose-free DMEM (Gibco) and exposed to 95% N₂ and 5% CO₂ for 12 h. Then, the glucose-free DMEM was replaced with normal DMEM, and the cells were returned to a normoxic chamber for 2 h of reoxygenation. TECs were treated in the presence or absence of NETs, degranulation substrate, DNase I (2 μ g/mL, Sigma), an MMP9 inhibitor (Sivelestat, 10 μ M, Selleck), an NE inhibitor (SB-3CT, 10 μ M, Selleck), an MPO inhibitor (MPO-IN-28, 10 μ M, Selleck), a TLR3 inhibitor (CU-CPT 4a, 10 μ M, MCE), poly(I: C) (MCE, 20 μ g/mL), or RNase III (40 U/mL, Thermo).

Western blotting

Protein was isolated using RIPA buffer (Sigma), supplemented with multiple protease inhibitors. Protein samples (15 μ g) were loaded, and after separation via 8–10% SDS-PAGE, the samples were transferred onto 0.22 μ m NC membranes. 5% BSA was used for blocking, and the membranes were then incubated overnight with antibodies against C-Caspase-1 (1:1000, CST), C-Caspase-3 (1:1000, CST), MLKL (1:1000, CST), P-MLKL (1:1000, CST) and β -Actin (1:1000, Proteintech).

Immunoprecipitation and LC-MS/MS

TECs were treated with NETs for 4 h. For immunoprecipitation, the cell lysates were incubated with magnetic beads containing an anti-J2 antibody specifically recognizing dsRNA (5 μ g). Magnetic beads containing IgG were used as a negative control. Following incubation, the samples were placed on a magnet to collect dsRNA-binding proteins. Proteins were sent to Shanghai Bio-profile Co. for further LC-MS/MS analysis. MaxQuant 1.6.1.0 was used to search a proteomics database.

Flow cytometry

Neutrophils from mouse bone marrow were activated with PMA, ionomycin or IRI-conditioned medium (CM) for 4–8 h. IRI-CM was prepared as we previously reported [14]. After treatment, the cells were washed with PBS, and fixed with 4% formaldehyde. 0.1% Triton X-100 was used for membrane permeabilization. Incubation with an anti-J2 antibody (1:100) followed by secondary antibody (Abcam, 1:200) was performed for intracellular staining. Flow cytometry was performed with a BD FACSCanto II.

Data availability

The RNA-seq data generated in this study will be disclosed in a public database before publication. The remaining data are available within the Article, Supplementary Information or available from the authors upon request.

Statistics

The data are presented as the means \pm standard deviations. All the statistical analyses were carried out using GraphPad Prism 8. One-way analysis of variance (ANOVA) and Tukey's test were used for the three or more group comparisons. Student's t test was used to compare the differences between two groups. A value of $P < 0.05$ was considered statistically significant.

Study approval

All animal experiments were conducted according to NIH Guide for the Care and Use of Laboratory Animals and the institutional guidelines of the Shanghai Jiao-tong University School of Medicine. All the procedures described were approved by the Animal Use and Care Committee of Shanghai Jiao Tong University School of Medicine.

Results

NETs are essential for aggravating inflammation in renal IRI

Neutrophils are a major contributor to inflammation; however, their specific involvement in renal IRI remains unclear. We observed that neutrophil infiltration was markedly increased in IRI model mice (Fig. 1A and Supplementary Figure S1A). To investigate the role of neutrophils in renal IRI, neutrophil-deficient *Csf3r*^{-/-} mice were used. We found that the serum creatinine (Cr) level (Fig. 1B) and degree of histological injury (Fig. 1C-D and Supplementary Figure S1B) were significantly lower in the *Csf3r*^{-/-} mice than in the WT mice. NETs are generated from neutrophils under inflammatory conditions, and play critical roles in manipulating inflammatory responses. We observed that NETs, which were represented by citrullinated histone H3 (CitH3), were generated in IRI model mice (Fig. 1D-E). Peptidylarginine deiminase 4 (PAD4) citrullinates histones and is required for the generation of NETs. The results revealed that NET formation was severely reduced in the kidneys of *Pad4*^{-/-} mice after IRI (Fig. 1D-E). In addition, the serum Cr concentration (Fig. 1B) and degree of histological injury (Fig. 1C-D and Supplementary Figure S1B) were reduced in *Pad4*^{-/-} mice. These findings indicate that neutrophil-induced tissue injury in renal IRI is associated with the generation of NETs.

Single-cell profiling of kidney cells from WT and *Pad4*^{-/-} mice subjected to IRI

To develop a comprehensive overview of the cellular and molecular changes associated with NETs in renal IRI, the transcriptomes of individual cells from WT and *Pad4*^{-/-} mice were analysed. After quality control filtering, we generated 44,133 single-cell transcriptomes, with 5448 cells in the WT sham group, 14,131 cells in the WT IRI group, 9268 cells in the *Pad4*^{-/-} sham group, and 15,266 cells in the *Pad4*^{-/-} IRI group. The cell populations were identified using unsupervised clustering and annotated on the basis of reported marker gene expression [17, 18]. UMAP plots revealed 16 cell clusters, including the PTs, the thick ascending limb of the loop of Henle in medulla (MTAL), the descending limb of the loop of Henle-thin ascending limb of the loop of Henle (DTL-ATL), the distal convoluted tubule (DCT), the distal convoluted tubule-connecting tubule (DCT-CNT), the type A intercalated cells of the collecting duct (ICA), the type B intercalated cells of the collecting duct (ICB), the urothelium (Uro), the podocyte (Pod), the pericyte (Per), the endotheliocyte (Endo), the monocyte (Mono), the macrophage (M ϕ), the neutrophil (Neu), the dendritic cell (DC), the B cell and the T cell clusters (Fig. 2A, Supplementary Figure S2 and Supplementary Table 1). The PT cluster contained the greatest proportions of cells in the kidney, and IRI further increased the PT proportion, which could be attributed to increased proliferation [18].

Aberrant immunocyte proportions were observed in the kidneys of IRI model mice. Among the immunocytes, the proportions of monocytes, macrophages, DCs, T cells and B cells were reduced, whereas the neutrophil proportion was apparently increased (Fig. 2B) in WT mice subjected to IRI, suggesting the essential role of neutrophils in renal IRI. Knockout of PAD4 alleviated the aberrant changes in the immunocyte composition (Fig. 2B). In addition, the PT injury markers *Havcr1* and *Krt20* were downregulated in *Pad4*^{-/-} mice (Fig. 2C). These findings suggest that neutrophil-derived NETs contribute to the PT injury in renal IRI.

Depletion of NETs alleviates PT injury in renal IRI model mice

PTs are highly heterogeneous, and the proximal tubule is more susceptible to damage because of its high metabolic activity. Unsupervised subclustering of PT cells and subsequent annotation revealed three healthy subclusters (the S1, S2, and S3 segments of the proximal tubule), and four injured subclusters (moderately injured PT S1-2, mildly injured PT S1-2, severely injured PT S1-2, and injured PT S3) (Fig. 3A). A cell trajectory analysis performed via Monocle validated the transition from healthy PT cells to injured PT cells (Fig. 3B). To characterize the functional features of different PT

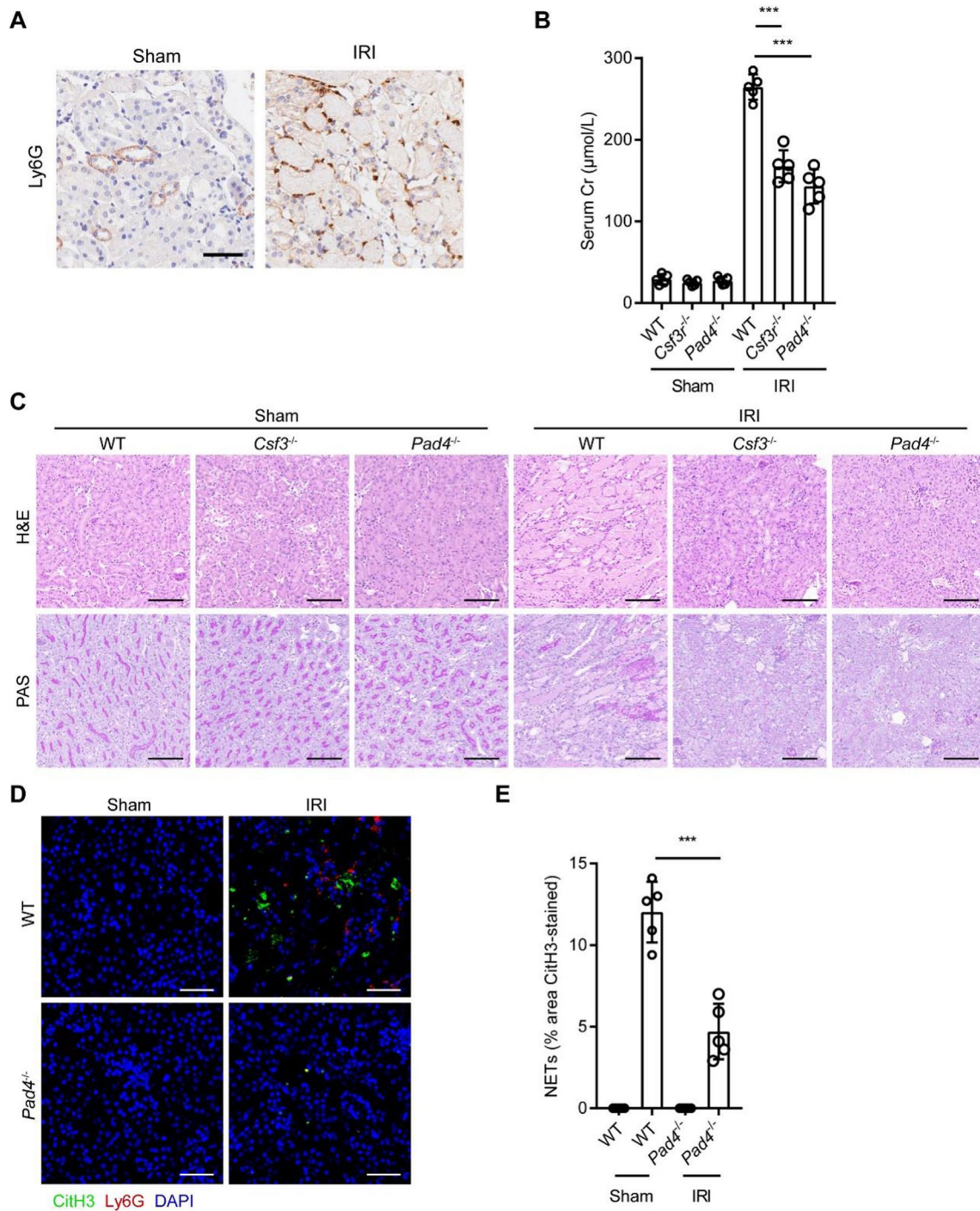


Fig. 1 NETs are essential for aggravating inflammatory responses in renal IRI. **(A)** Mice were subjected to IRI or sham surgery. Kidneys were collected and immunostained for Ly6G ($n = 5$ per group). The scale bar is 50 μm . **(B-C)** Wild-type (WT), *Csf3*^{-/-}, and *Pad4*^{-/-} mice were subjected to IRI or sham surgery. The level of creatinine (Cr) in the serum of IRI mice was determined **(B)** ($n = 5$ per group). H&E, and PAS staining were performed **(C)** ($n = 5$ per group). The scale bar is 100 μm . **(D-E)** WT and *Pad4*^{-/-} mice were subjected to IRI or sham surgery. Neutrophil extracellular traps (NETs) were assessed in the indicated groups by staining for citrullinated histone H3 (CitH3) (green), LY6G (red), and DAPI (blue) ($n = 5$ per group). The scale bar is 50 μm . *** $p < 0.001$, one-way ANOVA and Tukey's multiple comparisons test

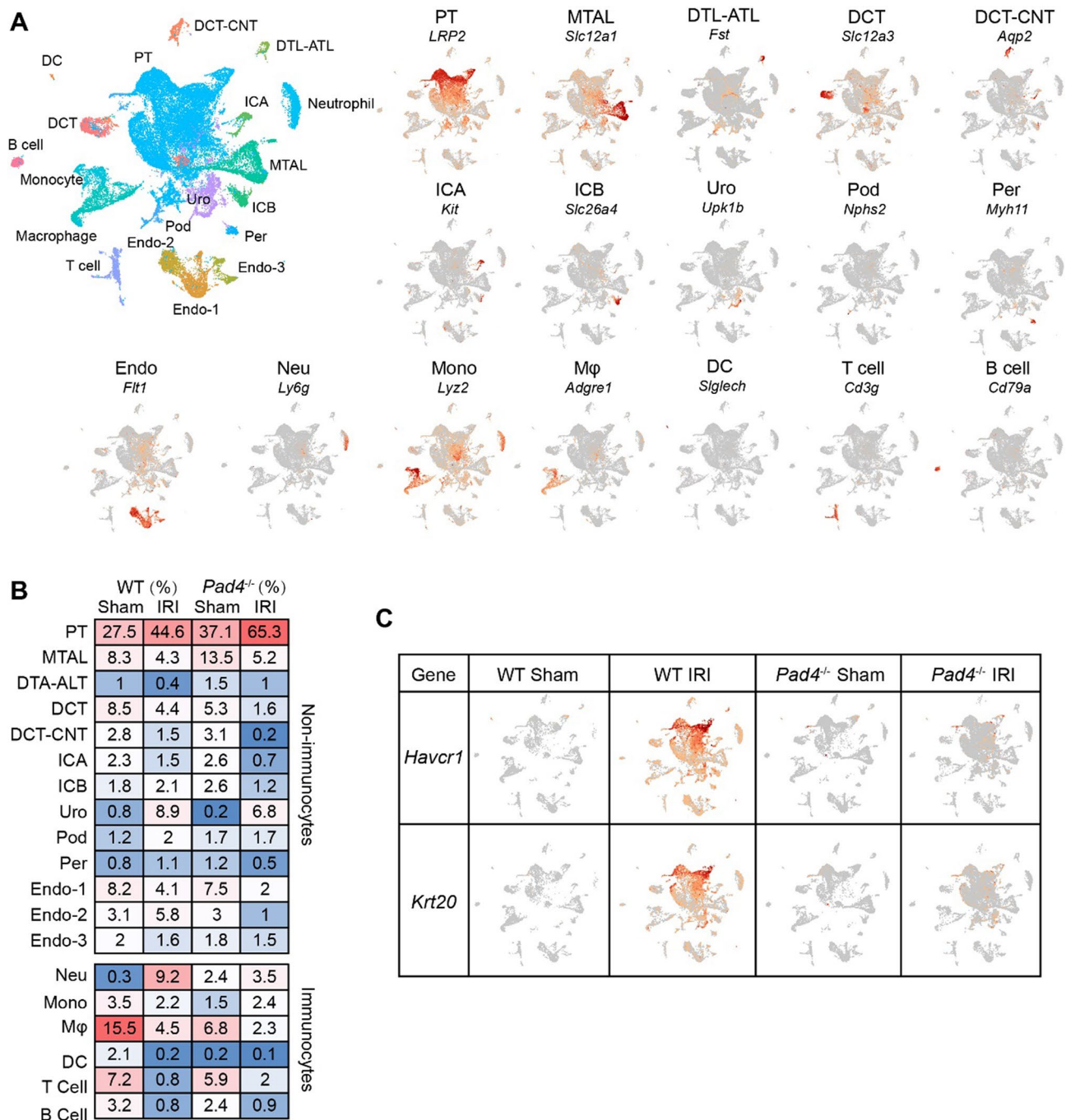


Fig. 2 Single-cell profiling of kidney cells from WT and *Pad4*^{-/-} mice subjected to IRI. **(A)** WT and *Pad4*^{-/-} mice were subjected to renal IRI or sham surgery. Single-cell RNA sequencing of kidney cells was performed (*n*=1 per group). UMAP plots of all kidney cells are displayed. Feature plots of different cell clusters in the kidney, including proximal tubular epithelial cells (PT), thick ascending limb of loop of Henle in medulla (MTAL), descending limb of loop of Henle-thin ascending limb of loop of Henle (DTL-ATL), distal convoluted tubule (DCT), distal convoluted tubule-connecting tubule (DCT-CNT), type A intercalated cells of collecting duct (ICA), type B intercalated cells of collecting duct (ICB), urothelium (Uro), podocytes (Pod), pericytes (Per), endothelial cells (Endo), monocytes (Mono), macrophages (Mφ), neutrophils (Neu), dendritic cells (DC), B cells and T cells. **(B)** Heatmap plots showing the proportions of different cell clusters in WT and *Pad4*^{-/-} mice. **(C)** Plots of genes of PT injury marker genes in WT and *Pad4*^{-/-} mice

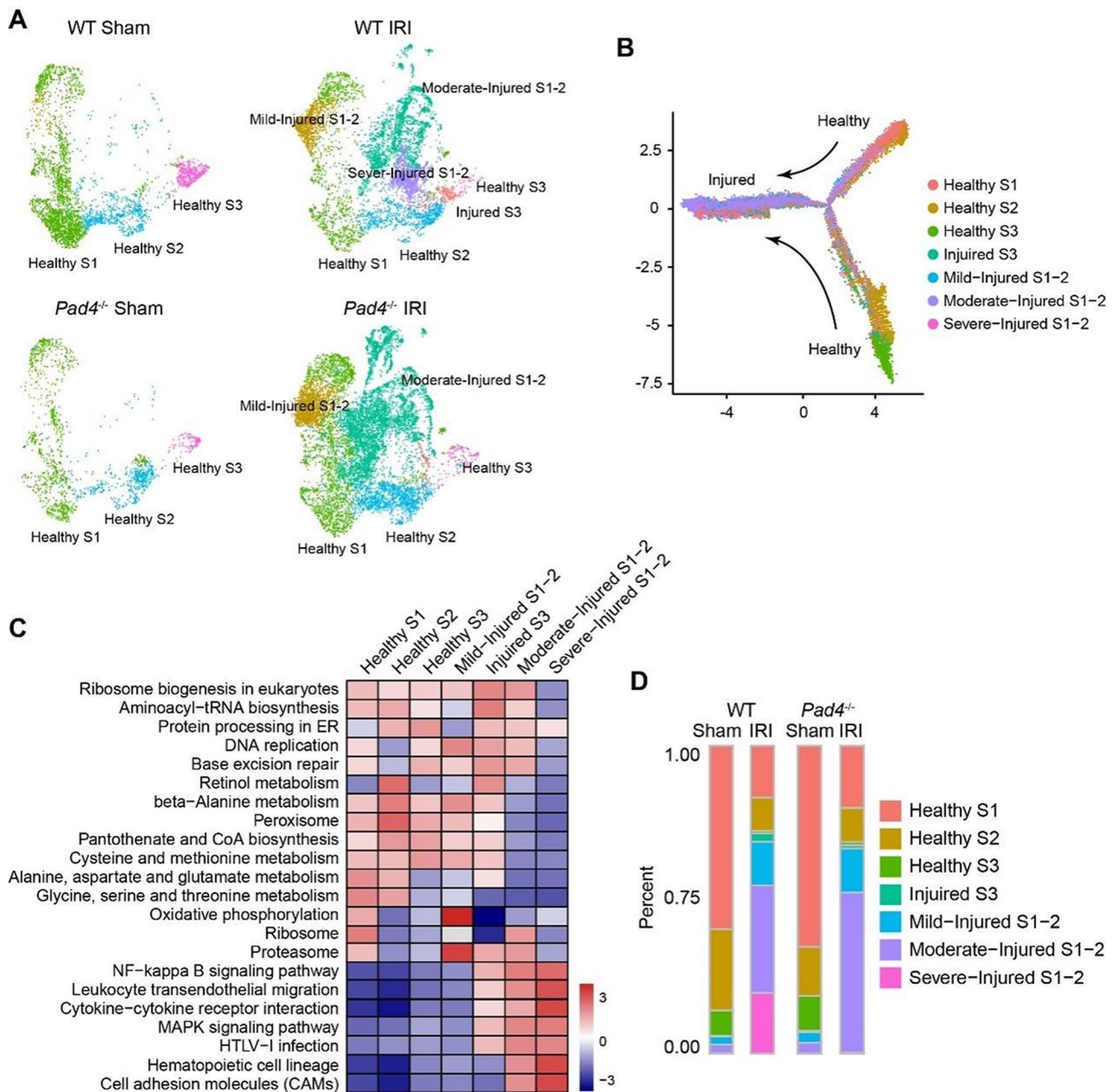


Fig. 3 Depletion of NETs alleviates renal PT injury in IRI. **(A)** WT and *Pad4*^{-/-} mice were subjected to renal IRI or sham surgery. Single-cell RNA sequencing of kidney cells was performed. UMAP plots of PTs from WT and *Pad4*^{-/-} mice are displayed. **(B)** Pseudotime trajectory of subclusters of PT colored by cluster identity. **(C)** GSEA of different PT subclusters was performed. Heatmap indicating the normalized enrichment score (NES). **(D)** Proportion of each PT subcluster in WT and *Pad4*^{-/-} mice

subclusters, gene set enrichment analysis (GSEA) functional analysis was performed (Fig. 3C). Pathways related to normal cell functions, including ribosome biogenesis, and cysteine and methionine metabolism, were enriched in healthy PTs, whereas inflammation-associated pathways, including cell adhesion molecules, MAPK signalling, cytokine-cytokine receptor interactions and the NF-κB signalling pathway, were enriched in injured PTs (Fig. 3C). PT S3 cells had the greatest expression of

inflammation-associated genes (Fig. 3C). By comparing the fractions of PT subclusters, we observed that mild-, moderate- and severely-injured PTs apparently accumulated in WT mice subjected to IRI (Fig. 3D). Depletion of NETs in *Pad4*^{-/-} mice eliminated most severely injured PT S1-2 and injured S3 cells, which further confirmed the role of NETs in PT injury (Fig. 3D).

NETs promote PT PANoptosis in renal IRI

PANoptosis is a form of inflammatory programmed cell death that exhibits key features of pyroptosis, apoptosis, and necroptosis. We detected enrichment of inflammation-associated pathways in injured PTs; however, whether PANoptosis is associated with inflammatory programmed cell death in renal IRI and potential NETs in this process remain unknown. Using the scRNA-seq, we analysed the pyroptosis score, apoptosis score, and necroptosis score of PTs according to the expression of specific genes (Table S2). The results revealed that the pyroptosis score, apoptosis score, and necroptosis score were increased in the PTs of renal IRI model WT mice (Fig. 4A). Interestingly, in *Pad4*^{-/-} mice, the pyroptosis, apoptosis, and necroptosis scores were reduced, indicating that PANoptosis was alleviated in NET-deficient mice (Fig. 4A). To confirm these results, immunohistochemical experiments were performed to analyse PANoptosis by examining the expression of cleaved Caspase-1 (pyroptosis), cleaved Caspase-3 (apoptosis), and phosphorylated mixed lineage kinase domain-like protein (P-MLKL) (necroptosis). Compared with that in sham mice, PANoptosis of PTs was apparently induced in WT IRI mice (Fig. 4B and S3A). However, in NET-deficient *Pad4*^{-/-} mice, PANoptosis was suppressed (Fig. 4B and S3A), suggesting the essential role of NETs in PTs PANoptosis. Using inhibitors of pyroptosis (disulfiram), apoptosis (Z-VAD-FMK) and necroptosis (necrosulfonamide) to block PANoptosis, we found that tissue injury (Fig. 4C and S3B) and the serum Cr concentration (Fig. 4D) were reduced, confirming the role of PANoptosis in the progression of renal IRI.

NET-induced RIPK1-PANoptosome induce PANoptosis in renal IRI

PANoptosis occurs in response to a variety of stimuli, including viral infection, gram-negative bacterial infection, and homeostatic perturbations. To respond to such diverse triggers, multiple PANoptosome sensors are needed to initiate programmed cell death. To date, three PANoptosome complexes with different sensors and regulators have been identified, namely the ZBP1-, AIM2- and RIPK1-PANoptosomes [6]. To investigate which PANoptosomes are associated with NET-induced PANoptosis in renal IRI, we evaluated the expression of *Zbp1*, *Aim2*, and *Ripk1* using scRNA-seq. The PTs predominantly expressed *Ripk1*, whereas *Zbp1* and *Aim2* were expressed mainly in immune cells (Fig. 5A). A similar expression pattern was also observed in a public scRNA-seq database (HPA) (Figure S4A), confirming the expression of *Ripk1* but not *Zbp1* or *Aim2* in PTs. Our scRNA-seq results, revealed that *Ripk1* expression in PTs was upregulated in renal IRI model WT mice, and that knockout of PAD4 reduced *Ripk1* expression (Fig. 5B).

Immunohistochemical studies also revealed that the upregulated expression of RIPK1 in PTs was reduced in *Pad4*^{-/-} mice, suggesting the potential involvement of RIPK1 in NET-induced PANoptosis (Fig. 5C). The role of RIPK1 in renal IRI was validated by treating mice with a specific RIPK1 inhibitor. The results showed that the RIPK1 inhibitor suppressed pyroptosis (indicated by cleaved Caspase-1), apoptosis (indicated by cleaved Caspase-3), and necroptosis (indicated by phosphorylated MLKL) in renal IRI mice (Fig. 5D and S4B). In addition, the RIPK1 inhibitor alleviated tissue injury (Fig. 5E and S4C) and reduced serum Cr (Fig. 5F) levels in renal IRI model mice, indicating that RIPK1-induced PANoptosis plays important roles in the pathological process of renal IRI.

NET-derived DsRNA triggers PANoptosis in renal IRI

The process of NET generation is concomitant with the release of abundant inflammatory stimuli, and the major bioactive substances include DNA, matrix metalloproteinase 9 (MMP9), neutrophil elastase (NE) and myeloperoxidase (MPO). We next explored which substance is essential for NET-induced PANoptosis. TECs were subjected to OGD/R to mimic renal IRI in vitro. We found that PANoptosis was moderately triggered in OGD/R-treated cells, as indicated by increased pyroptosis (indicated by cleaved GSDMD), apoptosis (indicated by cleaved Caspase-3), and necroptosis (indicated by phosphorylated MLKL) (Fig. 6A and S5A). NET stimulation further promoted PANoptosis in OGD/R-treated cells, whereas the degranulation medium of neutrophils failed to promote PANoptosis (Fig. 6A and S5A). DNA, MMP-9, NE, and MPO are considered the major bioactive substrates of NETs. Using DNase I or specific inhibitors to block the functions of these substrates, we found that PANoptosis was not alleviated (Fig. 6A and S5A). These findings suggest that other NET-derived substances might contribute to NET-induced PANoptosis.

Double-stranded RNA (dsRNA) is a potent inducer of inflammatory programmed cell death, and often accumulates during retroviral infection as a result of viral RNA replication [19]. Accumulating evidence has shown that dsRNA can be generated in eukaryotes under pathological conditions [19]. Our scRNA-seq results showed that the retroviral infection-associated “HTLV-1 infection” pathway and other inflammation-associated pathways were enriched in injured PT subclusters (Fig. 3C), whereas in NET-depleted *Pad4*^{-/-} mice, this enrichment was impaired (Figure S5B). These findings suggest that NET-associated dsRNA signalling may be involved in the induction of PANoptosis.

Using an anti-J2 antibody to detect dsRNA, we observed that the expression of dsRNA in unstimulated neutrophils was low, whereas dsRNA expression

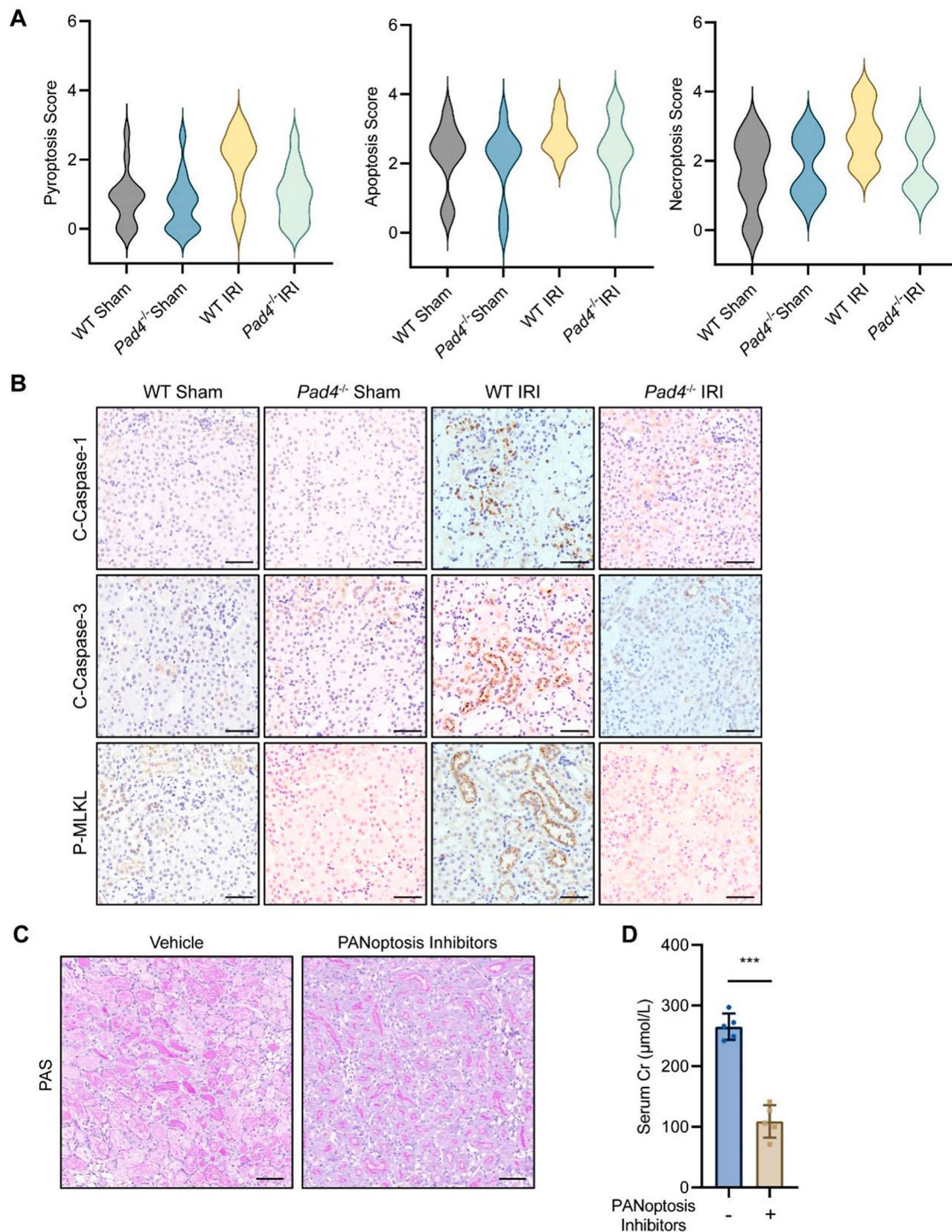


Fig. 4 NETs promote PT PANoptosis in renal IRI. **(A)** WT and *Pad4*^{-/-} mice were subjected to renal IRI or sham surgery. scRNA-seq of kidney cells was performed. Functional enrichment analysis was performed to compare pyroptosis scores, apoptosis scores, and necroptosis scores in PTs ($n=4$ per group). **(B)** WT and *Pad4*^{-/-} mice were subjected to renal IRI or sham surgery. Immunohistochemical staining was performed to assess the expression of cleaved Caspase-1 (C-Caspase-1), cleaved Caspase-3 (C-Caspase-3) and phosphorylated MLKL (P-MLKL). **(C and D)** WT mice were subjected to renal IRI surgery, in the presence or absence of PANoptosis inhibitors (a mixture of disulfiram, Z-VAD-FMK and necrosulfonamide). The kidney injury score was assessed by PAS staining ($n=4$ per group) **(C)**, and serum Cr levels ($n=5$ per group) **(D)**. *** $p < 0.001$, by Student's t test

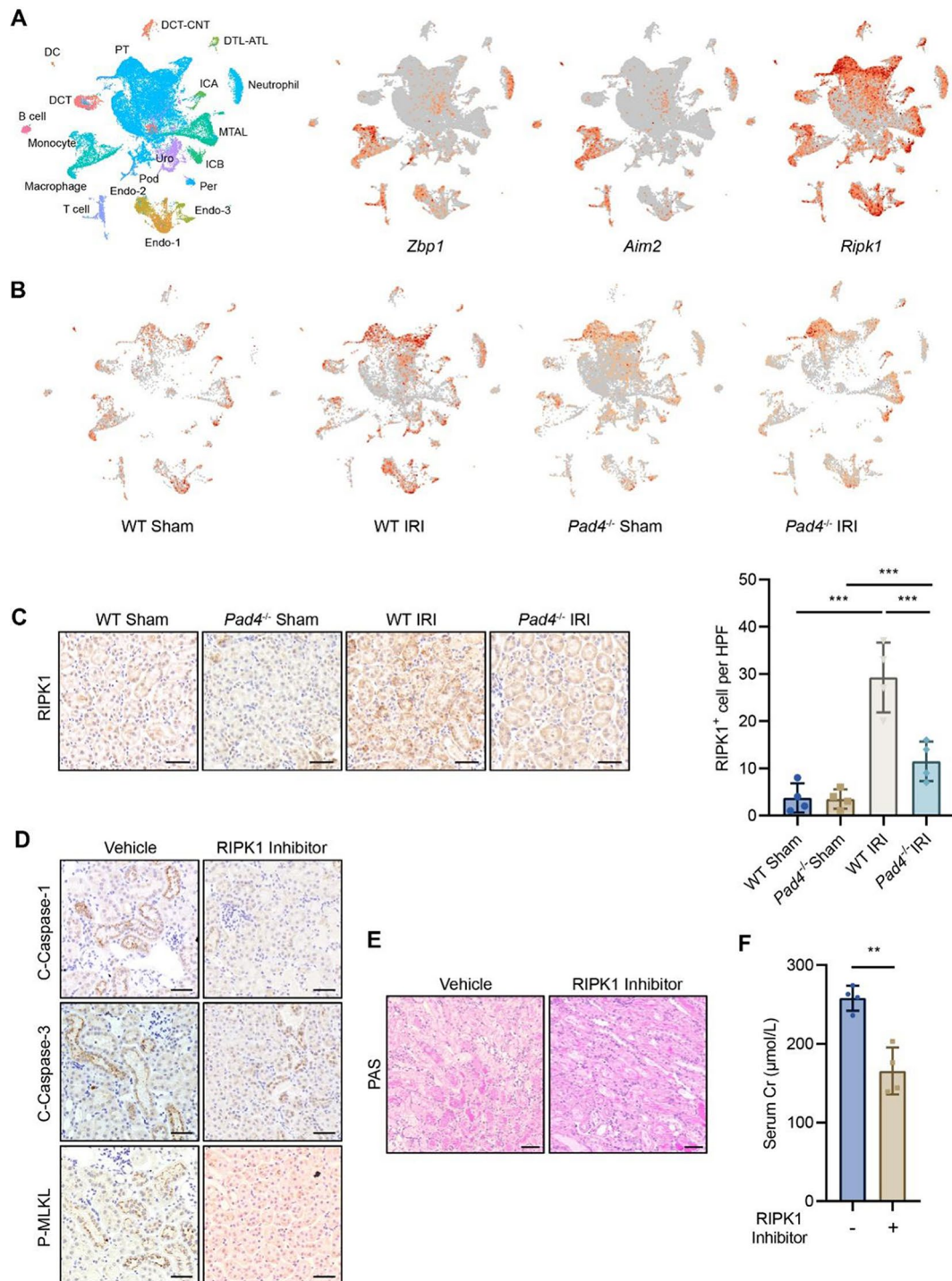


Fig. 5 NET-induced RIPK1-PANoptosomes execute PANoptosis in renal IRI. **(A)** WT and *Pad4*^{-/-} mice were subjected to renal IRI or sham surgery. scRNA-seq of kidney cells was performed. UMAP plots of all kidney cells are annotated, and *Zbp1*, *Aim2* and *Ripk1* expression is displayed. **(B)** UMAP plots showing *Ripk1* expression in the indicated mice are displayed. **(C)** WT and *Pad4*^{-/-} mice were subjected to renal IRI or sham surgery. Immunohistochemical staining was performed to assess RIPK1 expression ($n=4$ per group). **(D-F)** WT mice were subjected to renal IRI, in the presence or absence of a RIPK1 inhibitor (necrostatin 1 S). Immunohistochemical staining was performed to assess the expression of cleaved Caspase-1 (C-Caspase-1), cleaved Caspase-3 (C-Caspase-3) and phosphorylated MLKL (P-MLKL) ($n=4$ per group) **(D)**. Kidney injury was assessed by PAS staining ($n=4$ per group) **(E)**, and serum Cr levels ($n=4$ per group) **(F)**. * $p < 0.01$, *** $p < 0.001$, by one-way ANOVA and Tukey's multiple comparisons test **(C)**, or by Student's t test **(F)**

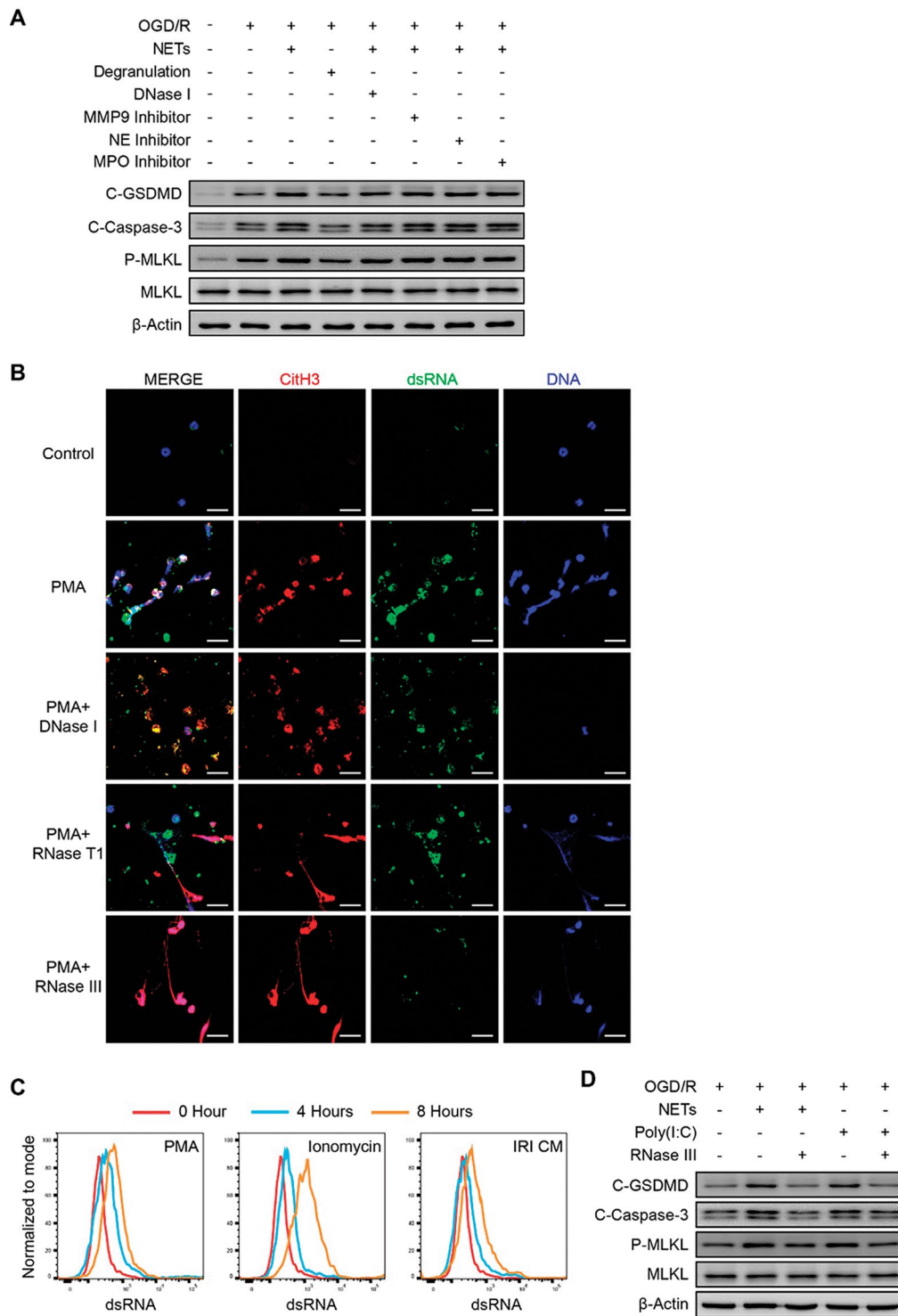


Fig. 6 NET-derived dsRNA triggers PANoptosis in renal IRI. **(A)** TECs were subjected to OGD/R in the presence or absence of NETs, degranulation substrate, DNase I, an MMP9 inhibitor, an NE inhibitor, and an MPO inhibitor. Western blotting was performed to assess the expression of cleaved GSDMD (C-GSDMD), cleaved Caspase-3 (C-Caspase-3) and phosphorylated MLKL (P-MLKL) ($n = 3$ per group). **(B)** NET formation was induced by phorbol 12-myristate 13-acetate (PMA). DNase I, RNase T1, or RNase III was used to treat NETs. The expression of CitH3, dsRNA and DNA was observed by confocal microscopy ($n = 6$ per group). **(C)** Neutrophils were activated with PMA, ionomycin or IRI conditional medium (CM) for 4–8 h. The level of intracellular dsRNA was assessed by flow cytometry ($n = 4$ per group). **(D)** TECs were treated with OGD/R in the presence or absence of NETs, poly(I:C), or RNase III. Western blotting was performed to assess the expression of C-GSDMD, C-Caspase-3 and P-MLKL ($n = 3$ per group)

markedly increased with the generation of NETs (Fig. 6B). Coexpression of extracellular dsRNA with DNA and CitH3 in NET-like structures was observed. The single-stranded RNA (ssRNA)-specific enzyme RNase T1 failed to degrade dsRNA, whereas the dsRNA-specific enzyme RNase III succeeded in degrading dsRNA (Fig. 6B), confirming the existence of dsRNA in NETs. In addition, when DNase I was used to degrade DNA, the dsRNA could still be coexpressed with CitH3 (Fig. 6B). To further confirm the expression of dsRNA in neutrophils, flow cytometry was performed to assess dsRNA expression. The results indicated that the NET-inducers PMA and ionomycin increased dsRNA expression at 4 h, and which was further enhanced at 8 h (Fig. 6C and S5C). In addition, the conditioned medium (CM) from IRI kidneys also enhanced dsRNA expression, confirming the expression of dsRNA in NETs in the context of renal IRI (Fig. 6C and S5C).

To assess the functional involvement of dsRNA in NET-induced PANoptosis, dsRNA-specific RNase III was used to treat OGD/R-treated cells. The results showed that RNase III inhibited PANoptosis in NET-stimulated cells (Fig. 6D and S5D). In addition, the synthetic analogue of dsRNA Poly(I: C) mimicked the effects of NETs which were abrogated by RNase III, verifying the role of dsRNA in PANoptosis (Fig. 6D and S5D).

NET-dsRNA-TLR3 signalling aggravates PANoptosis in renal IRI

To explore sensors of NET-derived dsRNA, dsRNA-binding proteins in TECs were immunoprecipitated and detected by targeted LC-MS/MS. The results showed that the RNA-binding proteins RBMX/RBMXL1 [20] and RBM39 [21], and the dsRNA-interacting proteins Annexin A2 [22] and EEF1A1 [23] were identified in anti-J2 antibody-immunoprecipitated substrates but not in IgG-immunoprecipitated substrates (Fig. 7A). dsRNA sensors include RIG-1, MDA5, LPG2, PKR, NLRP1, OAS and TLR3 [24]. Only TLR3 was identified by LC-MS/MS (Fig. 7A), suggesting the potential involvement of TLR3 in dsRNA sensing. Using the highly specific TLR3/dsRNA complex inhibitor CU-CPT 4a to treat NETs and poly(I: C)-stimulated cells, we found that PANoptosis was inhibited (Fig. 7B and S6A), indicating that the dsRNA/TLR3 pathway contributed to the PANoptosis. To assess whether in vivo inhibition of the NET-dsRNA-TLR3 pathway is effective in treating renal IRI, TLR3 inhibitors were used to treat IRI mice. The results showed that PANoptosis was suppressed by the TLR3/dsRNA complex inhibitor (Fig. 7C and S6B). In addition, alleviated kidney tissue injury (Fig. 7D and S6C) and decreased serum Cr levels (Fig. 7E) were also observed in RNase III- and TLR3 inhibitor-treated IRI mice. These findings

support the therapeutic potential of inhibiting the NET-associated dsRNA/TLR3 pathway in renal IRI.

Discussion

PANoptosis is a recently discovered inflammatory programmed cell death pathway, that integrates components of the pyroptosis, apoptosis and necroptosis pathways [5]. The total biological effects induced by PANoptosis cannot be accounted for by pyroptosis, apoptosis or necroptosis alone [25]. Therefore, compared with targeting a single programmed cell death pathway, targeting the PANoptosis pathway may have a more comprehensive therapeutic effect on renal IRI. The molecular events that regulate the PANoptosis process are complex, and involve interactions among hundreds of proteins [26]. Nevertheless, the formation of the PANoptosome is the key event to triggering PANoptosis [25]. To date, three PANoptosome complexes have been identified, namely, the ZBP1-, AIM2- and RIPK1-PANoptosomes [8]. Our scRNA-seq results showed that PTs predominantly expressed *Ripk1*. Further experiments indicated that the expression of RIPK1 in PTs was upregulated during renal IRI, and that the RIPK1 inhibitor succeeded in protecting against renal IRI. Targeting the RIPK1 PANoptosome may provide a potential target to preserve the function of PTs in renal IRI. In addition, we noted that *Ripk1* was also expressed in immune cells (mostly macrophages and monocytes) according to the seRNA-seq results. Previous studies have shown that RIPK1 PANoptosome assembly in macrophages is associated with the inflammatory cytokine storm and contributes to the death from severe infection [9]. It is speculated that the RIPK1 inhibitor used in renal IRI may also suppress PANoptosis and the inflammatory activation of macrophages, which protect against renal IRI.

DsRNA is usually associated with viral infection, as it constitutes the retroviral genome and can be generated in host cells during viral replication. Accumulating evidence suggests that dsRNA can also be generated from endogenous sources, such as retroelements, mitochondrial DNA and damaged DNA, in various pathophysiological states [27]. Given that mature neutrophils exhibit low dsRNA expression [28], and lack functional mitochondria [29], we speculate that NET-derived dsRNA is likely generated from damaged DNA, as the process of NET generation is characterized by neutrophil chromatin decondensation and DNA release. DsRNA is a potent inducer of inflammatory responses [30]. To date, RIG-1, MDA5, LPG2, PKR, NLRP1, OAS and TLR3 are recognized as the major sensors of dsRNA [24]. Most of these sensors are expressed intracellularly to sense intracellular dsRNA signals, possibly because viral infection occurs inside the cells [24]. A recent report revealed that endogenous dsRNA activated PKR to promote eIF2 α -dependent

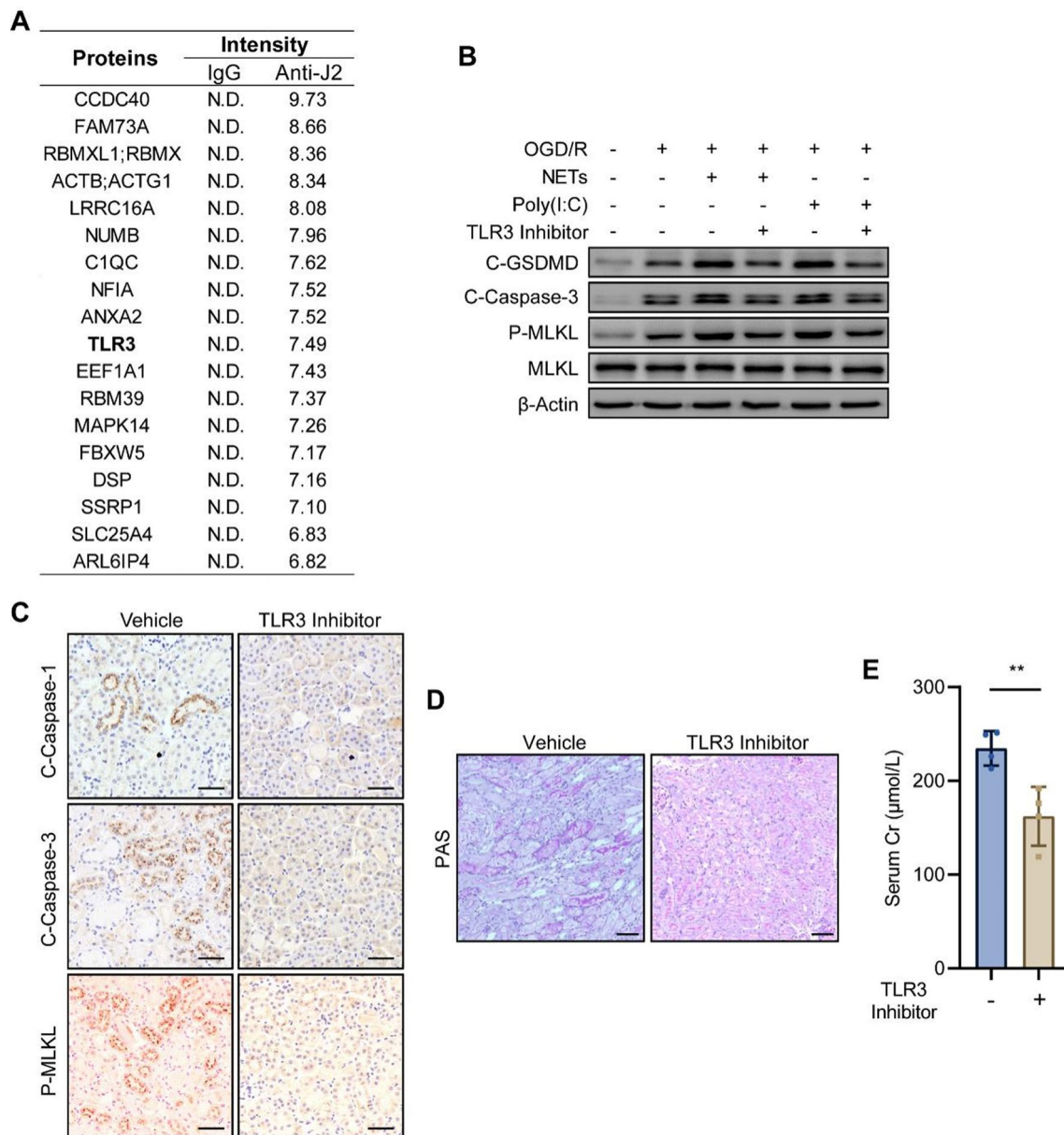


Fig. 7 NET-dsRNA-TLR3 signalling aggravates PANoptosis in renal IRI. **(A)** NETs were used to treat TECs. dsRNA-binding proteins were immunoprecipitated with an anti-J2 antibody and analysed via LC-MS/MS. IgG was used as a control ($n = 1$ per group). **(B)** TECs were treated with OGD/R in the presence or absence of NETs, poly (I: C) or a TLR3 inhibitor (CU-CPT 4a). Western blotting was performed to assess the expression of cleaved GSDMD (C-GSDMD), cleaved Caspase-3 (C-Caspase-3) and phosphorylated MLKL (P-MLKL) ($n = 3$ per group). **(C-E)** WT mice were subjected to renal IRI, in the presence or absence of a TLR3 inhibitor (CU-CPT 4a). Immunohistochemical staining was performed to assess the expression of C-Caspase-1, C-Caspase-3 and P-MLKL ($n = 4$ per group) **(C)**. Kidney injury scores were assessed by PAS staining ($n = 4$ per group) **(D)**, and serum Cr levels ($n = 4$ per group) **(E)**. ** $p < 0.01$ by Student's t test **(E)**

termination of general protein synthesis and promoted tubular injury [31]. This report also highlights the role of intracellular dsRNA signalling in renal tubular cells. As a pattern recognition receptor, TLR3 is expressed on the plasma membrane to sense extracellular dsRNA, which is strongly involved in inflammation-associated diseases [32]. In acute kidney injury, TLR3 signalling was found to be associated with inflammatory responses [33], and with the apoptosis and necrosis of renal tubules [34].

However, whether the dsRNA/TLR3 signalling axis contributes to renal IRI unknown. The present study expands the current understanding of the role of the dsRNA/TLR3 signalling axis in renal IRI by revealing that TLR3 is the main sensor of extracellular NET-derived dsRNA, and that the dsRNA/TLR3 signalling axis aggravates tissue injury in renal IRI by inducing PANoptosis pathways. In renal IRI, cellular damage may lead to the epigenetic dysregulation [35], aberrant RNA modification,

and defective RNA processing and degradation [36], all of which have been proven to generate endogenous dsRNA. In addition, mitochondrial damage during cellular stress may also lead to the formation of dsRNA structures [37]. We cannot exclude the possibility that dsRNA derived from damaged PTs may contribute to inflammatory PANoptosis in renal IRI by activating TLR3. It is hypothesized that a positive feedback loop mechanism may exist by which NET-derived dsRNA facilitates PT PANoptosis, and which leads to autocrine/paracrine release of dsRNA from injured PTs and subsequently aggravates PT PANoptosis and renal IRI. Chemical drugs targeting the dsRNA-TLR3 complex on the cell surface have achieved some effective results in asthma clinical trials [38]. These findings suggest that a cell-surface TLR3/dsRNA complex inhibitor is likely a potential therapeutic strategy for renal IRI.

Overall, the present study uncovers a mechanism by which NET/dsRNA/TLR3 signalling exacerbates PT cell PANoptosis in renal IRI. Therapies that target this pathway may be effective in treating renal IRI.

Supplementary Information

The online version contains supplementary material available at <https://doi.org/10.1186/s12964-025-02145-8>.

Supplementary Material 1

Supplementary Material 2: Fig. S1 NETs promote tissue injury in renal IRI. Fig. S2 Heatmap of the marker genes of each cell cluster identified on the basis of the single-cell RNA-seq data. Fig. S3 NETs promote PT PANoptosis in renal IRI. Fig. S4 NET-induced RIPK1-PANoptosome executes PANoptosis in renal IRI. Fig. S5 NET-derived dsRNA triggers PANoptosis in renal IRI. Fig. S6 TLR3 is the sensor of NET-derived dsRNA

Supplementary Material 3: Table S1 List of marker genes of determined from the scRNA-seq data.

Supplementary Material 4: Table S2 List of PANoptosis-associated genes.

Acknowledgements

This study was supported by the National Natural Science Foundation of China (ID 82270788 and 82470781 to Xiaodong Yuan).

Author contributions

Shaoyong Zhuang, Fangzhou Li, Liya Wang, Zilong Lai and Ming Zhang. Ruoyang Chen. Xianyun Zhang wrote the main manuscript text. Xiaodong Yuan provided the funding. All authors reviewed the manuscript.

Data availability

No datasets were generated or analysed during the current study.

Declarations

Competing interests

The authors declare no competing interests.

Author details

¹Department of Urology, Ren Ji Hospital, School of Medicine, Shanghai Jiao Tong University, 1630 Dongfang Road, Shanghai 200127, China

²Department of Urology, The Affiliated Huaian Hospital of Xuzhou Medical University, Jiangsu 223200, China

³Department of Urology, Jiading District Central Hospital Affiliated Shanghai University of Medicine & Health Sciences, Shanghai 201800, China

⁴Department of Nephrology, Kidney Research Institute, West China Hospital of Sichuan University, Chengdu 610041, China

Received: 18 September 2024 / Accepted: 8 March 2025

Published online: 17 March 2025

References

- Smith SF, Hosgood SA, Nicholson ML. Ischemia-reperfusion injury in renal transplantation: 3 key signaling pathways in tubular epithelial cells. *Kidney Int.* 2019;95:50–6.
- Linkermann A. Nonapoptotic cell death in acute kidney injury and transplantation. *Kidney Int.* 2016;89:46–57.
- Linkermann A, Skouta R, Himmerkus N, et al. Synchronized renal tubular cell death involves ferroptosis. *Proc Natl Acad Sci USA.* 2014;111:16836–41.
- Pefanis A, Ierino FL, Murphy JM, et al. Regulated necrosis in kidney ischemia-reperfusion injury. *Kidney Int.* 2019;96:291–301.
- Sun X, Yang Y, Meng X et al. PANoptosis: mechanisms, biology, and role in disease. *Immunol Rev* 2023.
- Chen W, Gullett JM, Tweedell RE, et al. Innate immune inflammatory cell death: PANoptosis and PANoptosomes in host defense and disease. *Eur J Immunol.* 2023;53:e2250235.
- Sundaram B, Pandian N, Mall R, et al. NLRP12-PANoptosome activates PANoptosis and pathology in response to Heme and pamps. *Cell.* 2023;186:2783–e28012720.
- Pandeya A, Kanneganti TD. Therapeutic potential of PANoptosis: innate sensors, inflammasomes, and RIPKs in PANoptosomes. *Trends in molecular medicine* 2023.
- Karki R, Sharma BR, Tuladhar S, et al. Synergism of TNF-alpha and IFN-gamma triggers inflammatory cell death, tissue damage, and mortality in SARS-CoV-2 infection and cytokine shock syndromes. *Cell.* 2021;184:149–e168117.
- Nemeth T, Sperandio M, Mocsai A. Neutrophils as emerging therapeutic targets. *Nat Rev Drug Discovery.* 2020;19:253–75.
- Ferhat M, Robin A, Giraud S, et al. Endogenous IL-33 contributes to kidney Ischemia-Reperfusion injury as an alarmin. *J Am Soc Nephrology: JASN.* 2018;29:1272–88.
- Papayannopoulos V. Neutrophil extracellular traps in immunity and disease. *Nat Rev Immunol.* 2018;18:134–47.
- Honda M, Kubes P. Neutrophils and neutrophil extracellular traps in the liver and Gastrointestinal system. *Nat Reviews Gastroenterol Hepatol.* 2018;15:206–21.
- Zhuang S, Xia S, Huang P, et al. Targeting P2RX1 alleviates renal ischemia/reperfusion injury by preserving mitochondrial dynamics. *Pharmacol Res.* 2021;170:105712.
- Raup-Konsavage WM, Wang Y, Wang WW, et al. Neutrophil peptidyl arginine deiminase-4 has a pivotal role in ischemia/reperfusion-induced acute kidney injury. *Kidney Int.* 2018;93:365–74.
- Zheng Z, Li C, Shao G, et al. Hippo-YAP/MCP-1 mediated tubular maladaptive repair promote inflammation in renal failed recovery after ischemic AKI. *Cell Death Dis.* 2021;12:754.
- Kirita Y, Wu H, Uchimura K, et al. Cell profiling of mouse acute kidney injury reveals conserved cellular responses to injury. *Proc Natl Acad Sci USA.* 2020;117:15874–83.
- Doke T, Abedini A, Aldridge DL, et al. Single-cell analysis identifies the interaction of altered renal tubules with basophils orchestrating kidney fibrosis. *Nat Immunol.* 2022;23:947–59.
- Chen YG, Hur S. Cellular origins of DsrRNA, their recognition and consequences. *Nat Rev Mol Cell Biol.* 2022;23:286–301.
- Prieto C, Nguyen DTT, Liu Z, et al. Transcriptional control of CBX5 by the RNA binding proteins RBM3 and RBM11 maintains chromatin state in myeloid leukemia. *Nat cancer.* 2021;2:741–57.
- Han T, Goralski M, Gaskill N et al. Anticancer sulfonamides target splicing by inducing RBM39 degradation via recruitment to DCAF15. *Science* 2017; 356.
- Zhang Q, Li S, Lei P, et al. ANXA2 facilitates enterovirus 71 infection by interacting with 3D polymerase and PI4KB to assist the assembly of replication organelles. *Virology.* 2021;36:1387–99.

23. Chen Z, Ye J, Ashraf U, et al. MicroRNA-33a-5p modulates Japanese encephalitis virus replication by targeting eukaryotic translation elongation factor 1A1. *J Virol*. 2016;90:3722–34.
24. Hur S. Double-Stranded RNA. Sensors and modulators in innate immunity. *Annu Rev Immunol*. 2019;37:349–75.
25. Lee S, Karki R, Wang Y, et al. AIM2 forms a complex with Pyrin and ZBP1 to drive PANoptosis and host defence. *Nature*. 2021;597:415–9.
26. Zheng M, Kanneganti TD. The regulation of the ZBP1-NLRP3 inflammasome and its implications in pyroptosis, apoptosis, and necroptosis (PANoptosis). *Immunol Rev*. 2020;297:26–38.
27. Sadeq S, Al-Hashimi S, Cusack CM et al., *Endogenous Double-Stranded RNA. Non-coding RNA* 2021; 7.
28. Khoyratty TE, Ai Z, Ballesteros I, et al. Distinct transcription factor networks control neutrophil-driven inflammation. *Nat Immunol*. 2021;22:1093–106.
29. Bodac A, Meylan E. Neutrophil metabolism in the cancer context. *Semin Immunol*. 2021;57:101583.
30. Paget M, Cadena C, Ahmad S, et al. Stress granules are shock absorbers that prevent excessive innate immune responses to DsRNA. *Mol Cell*. 2023;83:1180–e11961188.
31. Zhu Y, Zhang M, Wang W, et al. Polynucleotide phosphorylase protects against renal tubular injury via blocking mt-dsRNA-PKR-eIF2alpha axis. *Nat Commun*. 2023;14:1223.
32. Zhang X, Gao R, Zhang C, et al. Extracellular RNAs-TLR3 signaling contributes to cognitive impairment after chronic neuropathic pain in mice. *Signal Transduct Target Therapy*. 2023;8:292.
33. Hu X, Chen L, Li T, et al. TLR3 is involved in paraquat-induced acute renal injury. *Life Sci*. 2019;223:102–9.
34. Paulus P, Rupprecht K, Baer P, et al. The early activation of toll-like receptor (TLR)-3 initiates kidney injury after ischemia and reperfusion. *PLoS ONE*. 2014;9:e94366.
35. Chiappinelli KB, Strissel PL, Desrichard A, et al. Inhibiting DNA methylation causes an interferon response in cancer via DsRNA including endogenous retroviruses. *Cell*. 2015;162:974–86.
36. Liddicoat BJ, Piskol R, Chalk AM, et al. RNA editing by ADAR1 prevents MDA5 sensing of endogenous DsRNA as nonself. *Science*. 2015;349:1115–20.
37. Kim S, Lee K, Choi YS, et al. Mitochondrial double-stranded RNAs govern the stress response in chondrocytes to promote osteoarthritis development. *Cell Rep*. 2022;40:111178.
38. Silkoff PE, Flavin S, Gordon R, et al. Toll-like receptor 3 Blockade in rhinovirus-induced experimental asthma exacerbations: A randomized controlled study. *J Allergy Clin Immunol*. 2018;141:1220–30.

Publisher's note

Springer Nature remains neutral with regard to jurisdictional claims in published maps and institutional affiliations.